Transition Met Chem (2015) 40:839–846
DOI 10.1007/s11243-015-9980-8

Three discrete transition metal complexes of *N*-hydroxy-1,8-naphthalimidato ligand: synthesis, structure and magnetic properties

Chunmei Xia[1] · Shuang Wu[1] · Yuning Liang[1] · Zilu Chen[1] · Huahong Zou[1] · Fupei Liang[1,2]

Received: 30 July 2015 / Accepted: 10 September 2015 / Published online: 19 September 2015

Abstract The reactions of *N*-hydroxy-1,8-naphthalimide (HL) with $Mn(OAc)_2{\cdot}4H_2O$, $Co(NO_3)_2{\cdot}6H_2O$ and $CoCl_2{\cdot}6H_2O$ gave three new coordination compounds $[Mn_4(H_2O)_2L_6(OH)(OAc)]{\cdot}DMF{\cdot}6H_2O$ (**1**), $[Co_2(H_2O)_2L_4]{\cdot}2H_2O$ (**2**) and $[(CH_3)_2NH_2][Co(L)_2Cl]$ (**3**), the structures of which were determined. Compound **1** presents a parallelogram tetranuclear Mn_4 skeleton, and compound **2** shows a dinuclear structure. However, compound **3** has a mononuclear structure with the Co(II) center five-coordinated in a square-pyramidal geometry. The discrete units of the three compounds are linked by hydrogen bonds and π···π stacking interactions to form three-dimensional supramolecular frameworks. The magnetic data of **1** and **2** were collected and simulated in the temperature range of 2.0–300 K. These studies revealed the presence of two kinds of intramolecular antiferromagnetic interactions between the Mn(II) atoms in **1**, in contrast to intramolecular ferromagnetic interactions between the two Co(II) atoms in **2**, which are associated with the structural features.

Electronic supplementary material The online version of this article (doi:10.1007/s11243-015-9980-8) contains supplementary material, which is available to authorized users.

✉ Zilu Chen
zlchen@mailbox.gxnu.edu.cn

[1] School of Chemistry and Pharmaceutical Sciences, Guangxi Normal University, Guilin 541004, People's Republic of China

[2] College of Chemistry and Bioengineering, Guilin University of Technology, Guilin 541004, People's Republic of China

Introduction

The design and synthesis of discrete transition metal complexes have aroused great interest because of their intriguing architectures and topologies, as well as their potential applications as functional materials in the areas of magnetism, electrochemistry, luminescence and information storage [1–10]. As is well known, both coordination covalent bonds and weak non-covalent interactions such as hydrogen bonding and π···π stacking interactions contribute significantly in the formation of assemblies of discrete complexes. Thus the key point for the development of such compounds as magnetic materials is to design appropriate ligands bearing linking groups and non-coordinating groups with an idea of integrating both covalent and non-covalent interactions to give discrete complexes. The linking groups are to consolidate the metal atoms and thus to transmit the magnetic interactions between the adjacent paramagnetic metal atoms in the molecule [11–13]. The most used linking groups at present are oxo, hydroxide, oxime, carboxylate and so on [14]. The non-coordinating groups on the ligand also play a vital role in the magnetic propagation by adjusting the bridging modes of the linker and the M–O–M bridging angles. Moreover, the non-coordinating groups of the ligand are to control the nuclearity to obtain discrete structures [15], as well as to tune the intermolecular interactions for molecular stacking and intermolecular magnetic interactions [16, 17]. Thus the selection of proper non-coordinating groups on the ligands is also of great importance in constructing targeted magnetic materials.

Based on the above-mentioned considerations, we chose *N*-hydroxy-1,8-naphthalimide to make this investigation, which can be deprotonated to release *N*-hydroxy-1,8-naphthalimidato ligand. It has the capabilities of bridging

metal atoms to construct new structural patterns with diverse bridging modes through its three potential coordinating sites. In addition, its aromatic naphthalimide rings can provide $\pi\cdots\pi$ stacking interactions to sustain the supramolecular networks of discrete complexes. To the best of our knowledge, no studies were carried out to use *N*-hydroxy-1,8-naphthalimidato to consolidate metal atoms and to convey magnetic interactions between metal atoms in clusters. Thus we report here the structures of three new discrete complexes $[Mn_4(H_2O)_2L_6(OH)(OAc)]\cdot DMF\cdot 6H_2O$ (**1**), $[Co_2(H_2O)_2L_4]\cdot 2H_2O$ (**2**) and $[(CH_3)_2NH_2][CoL_2Cl]$ (**3**). The magnetic properties of **1** and **2** are discussed.

Experimental section

Materials and general methods

All reagents were used as obtained without further purification. The infrared spectra were recorded from KBr pellets in the range 4000–400 cm^{-1} with a PerkinElmer spectrum one FTIR spectrometer. Elemental analyses (C, H, N) were performed with a PerkinElmer 2400II CHN elemental analyzer. The powder X-ray diffraction (PXRD) data were collected with a Rigaku D/max 2500v/pc diffractometer with Cu-Kα radiation ($\lambda = 1.5418$ Å). All magnetic measurements were carried out on a Quantum Design MPMS-XL7 SQUID magnetometer. The experimental susceptibility data were corrected for the diamagnetic contribution calculated from Pascal constants, and the diamagnetism of the sample and sample holder was taken into account.

Synthesis of $[Mn_4(H_2O)_2L_6(OH)(OAc)]\cdot DMF\cdot 6H_2O$ (1)

To a 20-cm-long Pyrex tube containing $Mn(OAc)_2\cdot 4H_2O$ (0.025 mmol, 0.0062 g) and *N*-hydroxy-1,8-naphthalimide (0.025 mmol, 0.0053 g) was added DMF (0.5 mL), H_2O (0.5 mL) and NEt_3 (0.15 mL) in sequence. After being frozen by liquid nitrogen and subsequent evacuation, it was sealed, warmed and heated at 80 °C. Three days later, it was cooled slowly to ambient temperature over 1 day, yielding yellow crystals of **1**. These were collected, washed with a mixed solvent of DMF and H_2O followed by methanol, and finally dried at ambient temperature. Yield: 0.0027 g (36%, based on *N*-hydroxy-1,8-naphthalimide). Elemental Anal. Calcd. (%) for $C_{77}H_{63}N_7O_{30}Mn_4$: C, 51.8; H, 3.6; N, 5.5. Found: C, 51.7; H, 3.6; N, 5.8. IR (KBr, ν/cm^{-1}): 3206(w), 1664(m), 1637(s), 1586(s), 1386(s), 1288(s), 1250(m), 1233(w), 1082(w), 1043(m), 908(m), 842(w), 772(m), 725(w), 556(w).

Synthesis of $[Co_2(H_2O)_2L_4]\cdot 2H_2O$ (2)

To a 20-cm-long Pyrex tube containing $Co(NO_3)_2\cdot 6H_2O$ (0.025 mmol, 0.0073 g) and *N*-hydroxy-1,8-naphthalimide (0.025 mmol, 0.0053 g) was added DMF (0.5 mL), H_2O (0.5 mL) and NEt_3 (0.15 mL). After being frozen by liquid nitrogen and subsequent evacuation, it was sealed, warmed, and heated at 80 °C. Three days later, it was cooled slowly to ambient temperature, giving red crystals of **2**. These were collected by filtration, washed with a mixed solvent of DMF and H_2O followed by methanol, and finally dried at ambient temperature. Yield: 0.0017 g (26%, based on *N*-hydroxy-1,8-naphthalimide). Elemental Anal. Calcd. (%) for $C_{48}H_{32}N_4O_{16}Co_2$: C, 55.5; H, 3.1; N, 5.4. Found: C, 55.3; H, 3.2; N, 5.3. IR (KBr, ν/cm^{-1}): 2853(w), 1673(m), 1633(m), 1585(s), 1415(w), 1385(m), 1266(s), 1234(m), 1211(w), 1077(w), 1018(m), 898(m), 846(m), 775(m), 731(w), 564(w), 500(w).

Synthesis of $[(CH_3)_2NH_2][CoL_2Cl]$ (3)

To a 20-cm-long Pyrex tube containing $CoCl_2\cdot 6H_2O$ (0.1 mmol, 0.0119 g) and *N*-hydroxy-1,8-naphthalimide (0.1 mmol, 0.0213 g) was added DMF (0.5 mL), methanol (0.5 mL) and NEt_3 (0.15 mL) in sequence. After being frozen by liquid nitrogen and subsequent evacuation, it was sealed, warmed, and heated at 100 °C. Three days later, it was cooled slowly to ambient temperature over 1 day, giving red crystals of **3**. These were collected by filtration, washed with methanol and dried at ambient temperature. Yield: 0.0040 g (14%, based on *N*-hydroxy-1,8-naphthalimide). Elemental Anal. Calcd. (%) for $C_{26}H_{20}ClN_3O_6Co$: C, 55.3; H, 3.6; N, 7.4. Found: C, 55.2; H, 3.4; N, 7.7. IR (KBr, ν/cm^{-1}): 3035(w), 2790(w), 1692(m), 1631(w), 1592(s), 1463(w), 1384(m), 1258(m), 1233(m), 1211(w), 1023(m), 899(m), 845(w), 772(m), 549(w).

X-ray crystallography

Crystallographic data were collected with an Agilent Diffraction SuperNova (single source at offset) Eos diffractometer for complexes **1** and **3** and a Bruker SMART CCD diffractometer for complex **2** with graphite monochromated Mo-Kα radiation ($\lambda = 0.71073$ Å). Absorption correction was applied by using the multi-scan program SADABS [18]. The structures were solved by direct methods of SHELXS and were refined by full-matrix least-squares against F^2 using the SHELXL program in the SHELXTL package [19]. The location of the heaviest atoms was easily determined, and O, N and C atoms were subsequently determined from the difference Fourier maps. After all of the non-hydrogen atoms were located, the model was refined again, initially using isotropic and later anisotropic thermal displacement parameters. Hydrogen atoms attached on oxygen atoms were

located in a difference Fourier map and refined isotropically in the final refinement cycles. Other hydrogen atoms were placed in calculated positions and refined using a riding model. The acetate ligand in complex **1** shows some disorder with the methyl group on two positions, and with the acetate itself being just partially occupied on this position. The other parts on this position are one coordinated hydroxide ligand (O102) and two free water molecules (O112 and O152). The free DMF molecule is also disordered. Selected bond lengths and bond angles for complexes **1–3** are given in Tables S1–S3. A summary of crystallographic and structural refinement data for compounds **1–3** is given in Table 1.

Results and discussion

Synthesis and IR spectra

Complexes **1** and **2** were obtained from the reactions of *N*-hydroxy-1,8-naphthalimide (HL) with $Mn(OAc)_2{\cdot}4H_2O$ and $Co(NO_3)_2{\cdot}6H_2O$ in DMF and H_2O at 80 °C in the presence of NEt_3, respectively. Compound **3** was prepared from the reaction of cobalt(II) chloride with HL ligand in DMF and CH_3OH at 100 °C in the presence of NEt_3. To obtain pure samples in a reasonable yield, their synthetic conditions were optimized by varying the ratio of M^{2+}/HL, anions, reaction temperatures and solvents. The optimal synthetic conditions are presented in the experimental part. **1–3** could only be obtained in the given mixed solvents. Any attempts to use a single solvent such as DMF, H_2O, ethanol, methanol or other mixed solvents led to failure. Changing the anions of the metal salts for **1** or the ratio of the starting materials gave samples with much impurities and poor crystals.

The phase purities of the microcrystals of compounds **1–3** were confirmed by the nice agreement of experimental PXRD with those simulated from the single-crystal X-ray diffraction data (Figs. S1–S3, Supporting Information). The elemental analysis results of compounds **1–3** are in good agreement with the composition derived from the

Table 1 Crystallographic data of **1–3**

Complex	**1**	**2**	**3**
Formula	$C_{77}H_{63}Mn_4N_7O_{30}$	$C_{48}H_{32}N_4O_{16}Co_2$	$C_{26}H_{20}ClN_3O_6Co$
f_w	1786.10	1038.64	564.83
T/K	173(2)	296(2)	295(2)
λ/Å	0.71073	0.71073	0.71073
Crystal system	Monoclinic	Monoclinic	Monoclinic
Space group	$C2/c$	$P2_1/c$	$P2_1/c$
a/Å	24.8346(3)	16.588(3)	7.9247(2)
b/Å	13.6287(2)	15.335(3)	19.1223(6)
c/Å	21.5784(4)	16.823(3)	16.1990(6)
α/°	90	90.00	90.00
β/°	92.033(2)	94.513(3)	105.713(3)
γ/°	90	90.00	90.00
V/Å^3	7298.90(19)	4266.3(11)	2363.04(13)
Z	4	4	4
D_c/g cm^{-3}	1.625	1.617	1.588
μ/mm^{-1}	0.774	0.862	0.889
F(000)	3656	2120	1156
θ/°	2.99–25.01	1.23–26.46	3.19–26.99
Reflns collected	13,725	49,213	12,755
Reflns unique	6425	8791	5076
R_{int}	0.0213	0.0682	0.0389
GOF on F^2	1.068	1.033	1.153
R_1 $[I > 2\sigma(I)]$[a]	0.0515	0.0386	0.0557
wR_2 $[I > 2\sigma(I))]$[b]	0.1380	0.0896	0.0999
R_1 (all data)[a]	0.0648	0.0809	0.0750
wR_2 (all data)[b]	0.1496	0.1097	0.1072
Largest diff. peak, hole/(e Å^{-3})	0.757 and −0.415	0.548 and −0.452	0.367 and −0.279

[a] $R_1 = \Sigma||Fo| - |Fc||/\Sigma|Fo|$

[b] $wR_2 = [\Sigma w(Fo^2 - Fc^2)^2/\Sigma w(Fo^2)^2]^{1/2}$

single-crystal X-ray diffraction analysis. The IR spectra of **1–3** exhibit weak absorption bands at 3206, 2853 and 3035 cm^{-1}, respectively, which are assigned to the ν(OH) vibration of the coordinated water molecules [20, 21]. The bands at 898–909 and 1585–1692 cm^{-1} in the spectra of **1–3** are assigned to the ν(N–O) [22] and ν(C=O) [23, 24] of complexes **1–3**, respectively. The corresponding asymmetric ν(C=O) vibration in the spectrum of free *N*-hydroxy-1,8-naphthalimide (HL) ligand is at 1708 cm^{-1}. Obviously, the asymmetric ν(C=O) vibration bands in the three complexes are shifted, which suggests the coordination of the C=O groups to the metal atoms.

Crystal structures

The crystal structures of **1–3** were determined by single-crystal X-ray diffraction analysis. Selected bond lengths and angles are given in Tables S1–S3. A summary of crystallographic and structural refinement data for **1–3** is given in Table 1.

The single-crystal X-ray diffraction analysis revealed that per formula unit of complex **1** has one neutral discrete parallelogram tetranuclear molecule, six free water molecules and one free disordered DMF molecule. The four Mn(II) atoms are situated at the apexes of the parallelogram and are bridged by oxygen atoms (Fig. 1). All Mn(II) atoms in **1** are seven-coordinated. Among them, Mn1 and Mn1A are coordinated by three oxygen atoms from the N–O groups of three L^- ligands, three oxygen atoms from the C=O groups of three L^- ligands and another oxygen atom from the disordered OAc^- and OH^- ligands. Mn2 and Mn2A are coordinated by three oxygen atoms from the N–O groups of three L^- ligands, three oxygen atoms from the C=O groups of three L^- ligands and one oxygen atom from a water ligand. The coordination geometries of all Mn(II) atoms can be envisaged as distorted pentagonal bipyramidal with the distortion for Mn2 and Mn2A more severe than those of Mn1 and Mn1A. The Mn1–O and Mn2–O bond distances are in the range of 2.049(5)–2.437(3) and 2.128(3)–2.540(3) Å, respectively (Table S1). All L^- ligands in **1** behave as μ_2:η^4-bridges to link two Mn(II) atoms using their three oxygen atoms. Mn1 and Mn2, as well as Mn1A and Mn2A, are bridged by two L^- ligands. However, Mn1 and Mn2A (or Mn1A and Mn2) are bridged only by one L^- ligand. This leads to the consolidation of four Mn(II) atoms by six μ_2:η^4-bridging L^- ligands into a parallelogram skeleton with the Mn1–Mn2–Mn1A and Mn2–Mn1–Mn2A angles of 110.347(3) and 69.653(3)°, respectively. In the parallelogram skeleton, the Mn···Mn distances are 3.6022(2) Å for Mn1···Mn2 and 3.8356(2) Å for Mn1···Mn2A. Interestingly, the six L^- ligands in the tetranuclear unit are located in three planes. Two of them are nearly located in the parallelogram Mn4 plane. The remaining four L^- ligands form two planes parallel to each other with the aid of intramolecular $\pi\cdots\pi$ stacking interactions between the phenyl groups (centroid-to-centroid separation: 3.5351(1) Å, dihedral angle: 4.184(1)°). Hydrogen bonds (Table S4), as well as $\pi\cdots\pi$ stacking interactions, stabilize the whole structure of **1**, which is discussed in detail in the supporting information with the aid of some further figures (Figs. S4–S8).

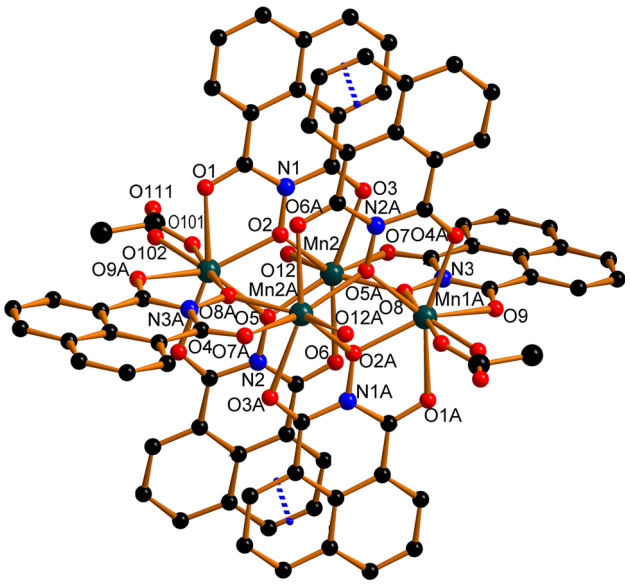

Fig. 1 Molecular structure of **1** with selected atoms labeled. C-bounded hydrogen atoms are omitted for clarity. *Blue broken lines* represent intramolecular $\pi\cdots\pi$ stacking interactions. Symmetry code: (A) $-x + 1/2, -y + 1/2, -z + 2$. (Color figure online)

The single-crystal X-ray diffraction analysis of complex **2** reveals two discrete dinuclear $[Co_2(L)_4(H_2O)_2]$ units in the structure as shown in Fig. 2. In addition, there are two uncoordinated water molecules per formula unit of complex **2**. All Co^{2+} atoms are six-coordinated in octahedral geometries completed by six oxygen atoms from three L^- ligands and one water ligand. The Co–O bond distances are in the range of 2.0174(19)–2.1506(19) Å (Table S2). Co1 and Co1A, as well as Co2 and Co2A, are connected by two oxygen atoms from the N–O groups of two L^- ligands with the Co–O–Co bond angles of 98.23(8)° and 97.84(8).

The neighboring binuclear $[Co_2(L)_4(H_2O)_2]$ units of **2** interact with each other through intermolecular hydrogen bonds O7–H7B···O12, O14–H14B···O2, O14–H14B···O3, O16–H16A···O4A, and O16–H16B···O8 (Table S5), as well as by $\pi\cdots\pi$ stacking interactions (centroid-to-centroid distance: 3.655(5) Å, dihedral angle: 3.263(1)°) between rings C4–C9 and C40–C45. This leads to the formation of supramolecular one-dimensional chains along the *a* direction (Fig. 3). Two adjacent one-dimensional supramolecular chains are linked by another water molecule (O15) through hydrogen bonds O15···O13 and O15···O16

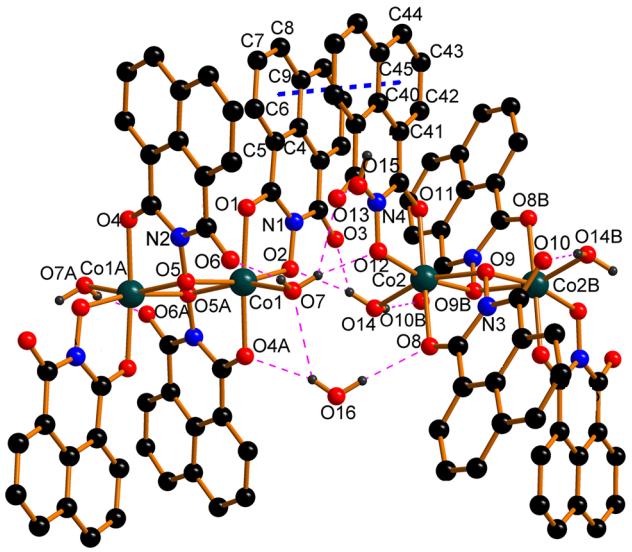

Fig. 2 Molecular structure of **2** with selected atoms labeled. *Thin* and *bold broken lines* indicate hydrogen bonds and $\pi\cdots\pi$ stacking interactions, respectively. C-bound hydrogen atoms are omitted for clarity. Symmetry codes: (A) $-x$, $-y$, $-z+1$, (B) $-x+1$, $-y$, $-z+1$. (Color figure online)

(symmetry code: x, $-y+1/2$, $z-1/2$) as shown in Fig. S9 and by $\pi\cdots\pi$ stacking interaction (Fig. S10, centroid-to-centroid distance: 3.764(2) Å, dihedral angle: 6.781(4)°) between naphthalene rings C15–C24 and C3–C12 (symmetry code: $-x$, $0.5+y$, $0.5-z$). This results in the connection of each one-dimensional supramolecular chain with another four ones to form a supramolecular structure (Fig. S11).

Complex **3** presents a mononuclear anion of $[Co(L)_2Cl]^-$ (Fig. 4) and a cation of $[(CH_3)_2NH_2]^+$. The Co(II) atom in **3** is five-coordinated in a distorted square-pyramidal coordination geometry by four oxygen atoms from two L^- ligands and one chloride anion. The Co–O bond lengths and O–Co1–O bond angles in **3** are in the ranges of 1.952(2)–2.138(2) Å and 78.48(9)-157.53(9)° (Table S3), respectively. The Co–Cl bond length of **3** is 2.2733(10) Å,

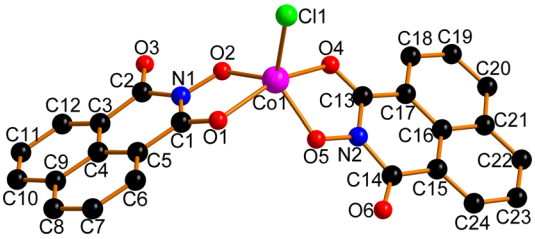

Fig. 4 Molecular structure of **3** with atoms labeled. H atoms on the carbon atoms are omitted for clarity. (Color figure online)

and the O–Co(1)–Cl bond angles in **3** are in the ranges of 100.96(7)–120.48(7)°. The mononuclear units in the *a* direction are linked by $[(CH_3)_2NH_2]^+$ cations through hydrogen bonds N3–H3A···O5, N3–H3A···O6, N3–H3B···O2A and N3–H3B···O3A (Table S6) to form supramolecular one-dimensional chains (Fig. 5). Each mononuclear unit interacts with another three ones by $\pi\cdots\pi$ stacking interactions between rings C15, C16, C21–C24 and N1, C1–C5 (x, $0.5-y$, $0.5+z$), and rings N1, C1–C5 and C15, C16, C21–C24 (x, $0.5-y$, $-0.5+z$) with a center-to-center distance of 3.3942(1) Å, a dihedral angle of 14.023° and offset angles of 4.968(1) and 13.595°, as well as between rings N1, C1–C5 and C4–C9 ($1-x$, $1-y$, $-z$), C4–C9 and N1, C1–C5 ($1-x$, $1-y$, $-z$) with a center-to-center distance of 3.4982(1) Å, a dihedral angle of 1.452° and an offset angles of 18.714(1) and 20.154(2)°. These $\pi\cdots\pi$ stacking interactions result in the connection of each 1D H-bonded supramolecular chain with another three ones, leading to the construction of a three-dimensional supramolecular structure (Fig. S12).

Apparently, the reactions of *N*-hydroxy-1,8-naphthalimide (HL) with $Mn(OAc)_2{\cdot}4H_2O$, $Co(NO_3)_2{\cdot}6H_2O$ and $CoCl_2{\cdot}6H_2O$ gave three complexes with different structures. Complex **1** presents a parallelogram tetranuclear Mn_4 skeleton. However, complexes **2** and **3** show only dinuclear and mononuclear structures, respectively. The anions in the transition metal salts used for the preparation of **1** and **3** participate in the coordination to metal atoms in

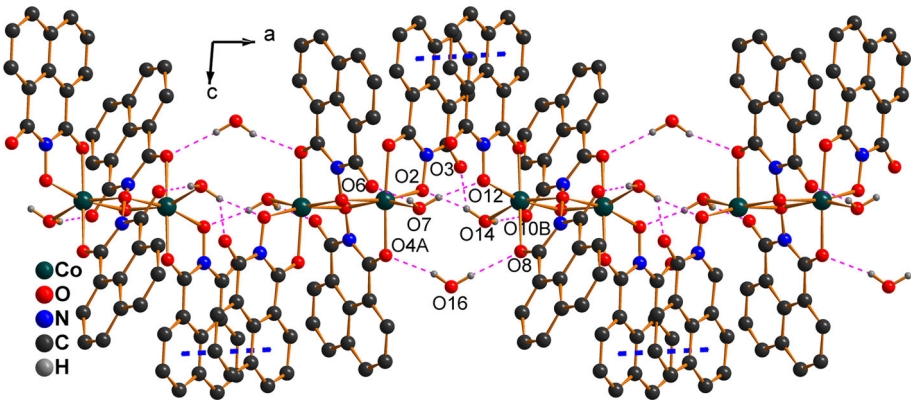

Fig. 3 Supramolecular chain of **2** formed by hydrogen bonds (*thin broken lines*) and $\pi\cdots\pi$ stacking interactions (*bold broken lines*). H atoms on the carbon atoms are omitted for clarity. Symmetry codes: (A) $-x$, $-y$, $-z+1$, (B) $-x+1$, $-y$, $-z+1$. (Color figure online)

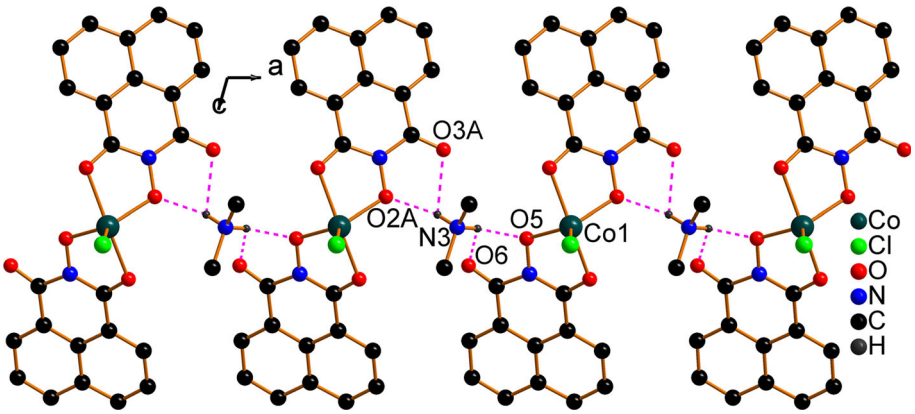

Fig. 5 Supramolecular chain of **3** formed by hydrogen bonds. H atoms on the carbon atoms are omitted for clarity. Symmetry code: (A) $x - 1, y, z$. (Color figure online)

monodentate modes. The L^- ligands in the three complexes adopt different coordination modes as shown in Scheme 1. All L^- ligands in **1** and **3** behave as μ_2-chelating:chelating (Scheme 1a) and chelating (Scheme 1c) coordination modes, respectively. However, the L^- ligands in **2** have both μ_2-chelating:bridging (Scheme 1b) and chelating (Scheme 1c) coordination modes. Based on the full comparison of the starting materials and the reaction conditions in the preparation of these complexes, the difference in the structure for **1** from those for **2** and **3** is probably mainly due to the different transition metal atoms used in the preparation. The structural difference for **2** and **3** might be ascribed to the different anions in the Co(II) salts used in their preparation. It reveals the role of different transition metal atoms and anions in the formation of different structures.

Magnetic properties

The variable-temperature magnetic susceptibilities of **1** and **2** were measured in an applied magnetic field of 1000 Oe in the temperature range of 2–300 K. Figures 6 and 7 show the $\chi_m T$ and χ_m vs T plots for complexes **1** and **2**, respectively, in which the χ_m is the molar magnetic susceptibility.

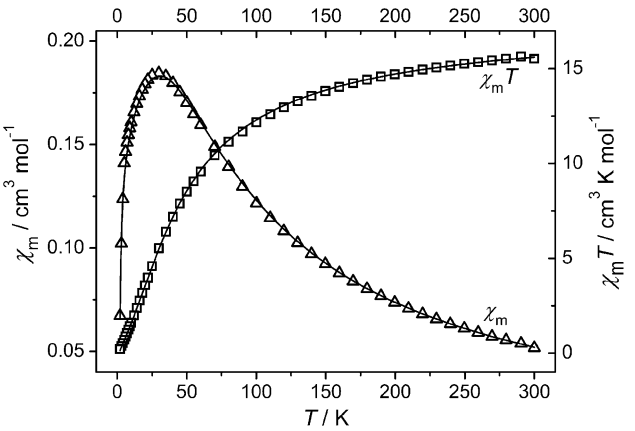

Fig. 6 Plots of χ_m and $\chi_m T$ versus T for **1**

The temperature-dependent magnetic susceptibilities of **1** reveal a $\chi_m T$ value of 15.52 cm^3 K mol^{-1} at 300 K, which is lower than the calculated value of 17.51 cm^3 K mol^{-1} for four magnetically isolated Mn^{2+} atoms. The $\chi_m T$ value gradually decreases upon decreasing temperature from 300 K and reaches a minimum value of 0.21 cm^3 K mol^{-1} at 2 K. The behavior of the magnetic susceptibility above 60 K obeys the Curie–Weiss rule, with

Scheme 1 A schematic show of the coordination modes of L^- ligands in **1–3**

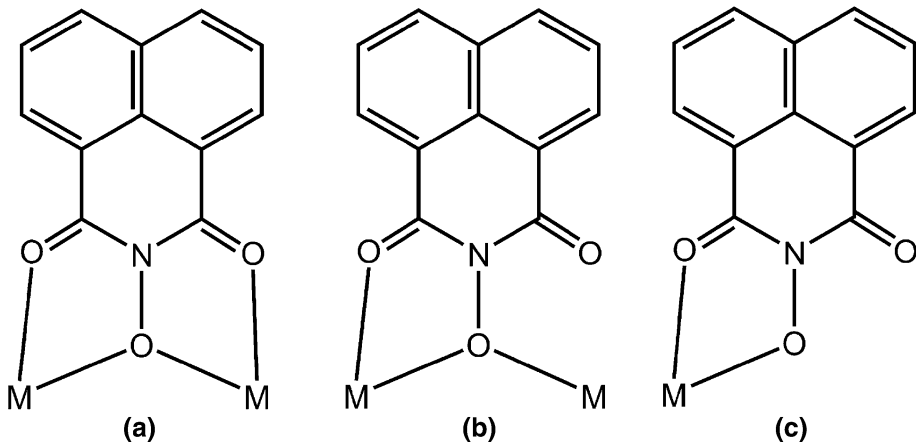

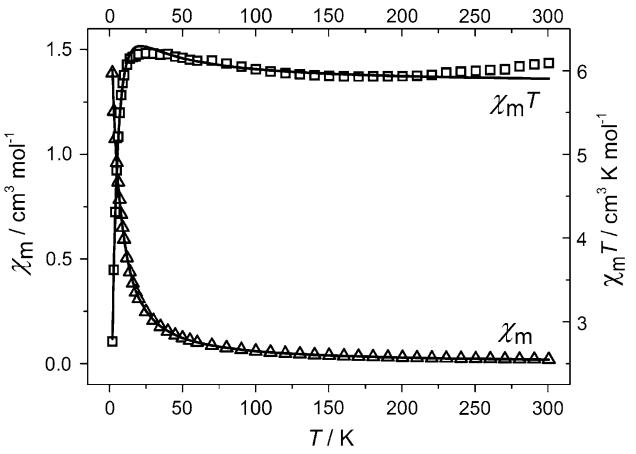

Fig. 7 Plots of χ_m and $\chi_m T$ versus T for **2**

$C = 18.40$ cm^3 K mol^{-1} and $\theta = -51.40$ K. The nature of the $\chi_m T$ versus T plot and the negative θ value indicate possible antiferromagnetic coupling between Mn^{2+} atoms. The structural analysis of **1** revealed a parallelogram skeleton with two kinds of magnetic exchange pathways as shown in Scheme 2. The Mn1···Mn2 and Mn1A···Mn2A magnetic interactions are mediated by two μ-oxo bridges with the Mn–O–Mn angles of 112.42(17) and 113.43(18)° and the Mn···Mn distance of 3.602(2) Å. However, the Mn1···Mn2A and Mn1A···Mn2 magnetic interactions are mediated by one μ-oxo bridge with the Mn–O–Mn angles of 126.82(15)° and the Mn···Mn distance of 3.834(2) Å. The above-mentioned magnetic exchange model can give the Hamiltonian in Eq. (1).

$$\hat{H} = -2J_1\left(\hat{S}_1\hat{S}_2 + \hat{S}_{1A}\hat{S}_{2A}\right) - 2J_2\left(\hat{S}_1\hat{S}_{2A} + \hat{S}_{1A}\hat{S}_2\right) \quad (1)$$

The simulation of the experimental magnetic data of **1** using the MagPack program [25] gives a nice agreement to the experimental data with the following parameters: $g = 2.00$, $J_1 = -3.01$ cm^{-1}, $J_2 = -1.00$ cm^{-1}. The negative exchange interactions confirm again the presence of antiferromagnetic interactions between the Mn(II) atoms in **1**, which is also consistent with the correlation between the J value and the Mn–O–Mn angle [26, 27].

The measured $\chi_m T$ value of complex **2** per two Co(II) atoms at 300 K is 6.09 cm^3 K mol^{-1}, which is much larger

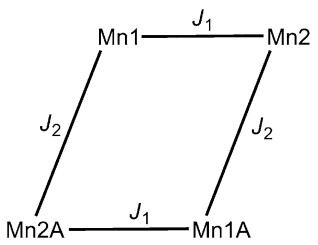

Scheme 2 Magnetic exchange pathways for **1**

than the spin-only value (3.75 cm^3 K mol^{-1}) for two magnetically isolated high-spin Co(II) atoms, probably due to the contribution of unquenched orbital momentum [28]. With the decrease in the temperature, $\chi_m T$ first decreases slightly from 300 to 170 K. Upon further cooling, it rises up and reaches a maximum value of 6.21 cm^3 K mol^{-1} at 25 K and subsequently decreases again to 2.61 cm^3 K mol^{-1} at 2 K. Between 2 and 300 K, the magnetic susceptibilities can be fit to the Curie–Weiss rule with $C = 6.01$ cm^3 K mol^{-1} and $\theta = -0.26$ K. As stated in the structural discussion, **2** presents a discrete dinuclear skeleton with the two Co(II) atoms linked by two μ-oxo bridges in a Co···Co separation of 3.1781(5) and 3.1869(5) Å. The Co–O–Co angles are 97.84(8) and 98.23(8)°, which are assumed to give rise to weakly ferromagnetic interaction as described previously [29, 30]. To confirm this, the experimental magnetic data were simulated using a dinuclear model based on the spin Hamiltonian $\hat{H} = -2J\hat{S}_1\hat{S}_2$ [31, 32], giving fitting parameters $g = 2.49$, $J = 1.94$ cm^{-1}, $zJ = -0.41$ cm^{-1}, $R = 7.32 \times 10^{-5}$. The positive J value demonstrates ferromagnetic interaction between the two Co(II) atoms in **2**. Thus the decrease in χ_mT upon cooling in the temperature range of 300–170 K might be ascribed to the effect of several factors: the contribution of the orbital angular momentum, intermolecular antiferromagnetic coupling, single-ion behavior of Co(II), and the depopulation of the higher energy spin-orbital levels [30, 33, 34].

Conclusion

With the aim of preparing discrete complexes, *N*-hydroxy-1,8-naphthalimide was selected as ligand in this work for its bridging group fused on the non-coordinating aromatic naphthalimide group. Its coordination to Mn(II) and Co(II) atoms provides three new discrete complexes. **1** shows a parallelogram tetranuclear Mn_4 skeleton with two kinds of Mn···Mn connections. **2** and **3** show dinuclear and mononuclear structures, respectively. The rich intramolecular and intermolecular hydrogen bonds and $\pi\cdots\pi$ stacking interactions in these compounds were analyzed in detail in the formation of their supramolecular structures. The collected magnetic data of **1** were simulated based on the parallelogram tetranuclear Mn_4 model, which reveals two kinds of intramolecular Mn···Mn antiferromagnetic interactions. There is intramolecular ferromagnetic interaction between the two Co(II) atoms in **2**, as demonstrated by the experimental and fitted magnetic data. Their magnetic properties are associated with their structural features. The further exploration of high nuclearity clusters using *N*-hydroxy-1,8-naphthalimidato ligand is under way in our group.

Supplementary material

CCDC 1049531, 1049532 and 1049533 contain the supplementary crystallographic data for **1**, **2** and **3**, respectively. These data can be obtained free of charge on quoting the depository numbers via http://www.ccdc.cam.ac.uk/conts/retrieving.html or from the Cambridge Crystallographic Data Centre, 12 Union Road, Cambridge CB2 1EZ, UK; fax: (+44) 1223-336-033; or e-mail: deposit@ccdc.cam.ac.uk.

Acknowledgments The authors thank the financial support by National Natural Foundation of China (Grant No. 21261004), Guangxi Natural Science Foundation of China (Grant Nos. 2013GXNSFGA019008 and 2013GXNSFAA019039) and Program for Excellent Talents in Guangxi Higher Education Institutions.

References

1. Wang X-Y, Avendano C, Dunbar KR (2011) Chem Soc Rev 40:3213–3238
2. Ohkoshi S-I, Imoto K, Tsunobuchi Y, Takano S, Tokoro H (2011) Nat Chem 3:564–569
3. Liu T, Zhang Y-J, Wang Z-M, Gao S (2008) J Am Chem Soc 130:10500–10501
4. Singh D, Baruah JB (2012) Cryst Growth Des 12:2109–2121
5. Reger DL, Derek Elgin J, Pellechia PJ, Smith MD, Simpson BK (2009) Polyhedron 28:1469–1474
6. Nath JK, Mondal A, Powell AK, Baruah JB (2014) Cryst Growth Des 14:4735–4748
7. Garcia-Bueno R, Santana MD, Sanchez G, Garcia J, Garcia G, Perez J, Garcia L (2010) Dalton Trans 39:5728–5736
8. Licchelli M, Biroli AO, Poggi A, Sacchi D, Sangermani C, Zema M (2003) Dalton Trans 4537–4545
9. Mukherjee S, Mukherjee PS (2014) Cryst Growth Des 14:4177–4186
10. Díaz-Gallifa P, Fabelo O, Pasán J, Cañadillas-Delgado L, Rodríguez-Carvajal J, Lloret F, Julve M, Ruiz-Pérez C (2014) Inorg Chem 53:5674–5683
11. Wang X-Y, Wang L, Wang Z-M, Gao S (2005) J Am Chem Soc 128:674–675
12. Mukherjee P, Drew MGB, Gómez-García CJ, Ghosh A (2009) Inorg Chem 48:4817–4827
13. Zeng M-H, Zhang W-X, Sun X-Z, Chen X-M (2005) Angew Chem Int Ed 44:3079–3082
14. Sharma AK, Lloret F, Mukherjee R (2013) Inorg Chem 52:4825–4833
15. Reger DL, Pascui AE, Smith MD, Jezierska J, Ozarowski A (2012) Inorg Chem 51:11820–11836
16. Reger DL, Horger JJ, Debreczeni A, Smith MD (2011) Inorg Chem 50:10225–10240
17. Reger DL, Debreczeni A, Smith MD, Jezierska J, Ozarowski A (2011) Inorg Chem 51:1068–1083
18. Sheldrick GM (2002) SADABS, 2.05th edn. University of Göttingen, Germany
19. Sheldrick GM (1997) SHELXTL NT, 5.1st edn. University of Göttingen, Germany
20. Arauzo A, Lazarescu A, Shova S, Bartolome E, Cases R, Luzon J, Bartolome J, Turta C (2014) Dalton Trans 43:12342–12356
21. Biswas R, Mukherjee S, Kar P, Ghosh A (2012) Inorg Chem 51:8150–8160
22. Chen Z, Jia M, Zhang Z, Liang F (2010) Cryst Growth Des 10:4806–4814
23. Reger DL, Debreczeni A, Smith MD (2011) Inorg Chem 50:11754–11764
24. Croitor L, Coropceanu EB, Jeanneau E, Dementiev IV, Goglidze TI, Chumakov YM, Fonari MS (2009) Cryst Growth Des 9:5233–5243
25. Borrás-Almenar JJ, Clemente-Juan JM, Coronado E, Tsukerblat BS (2001) J Comput Chem 22:985–991
26. Sun C-Y, Gao S, Jin L-P (2006) Eur J Inorg Chem 2006:2411–2421
27. Gultneh Y, Tesema YT, Yisgedu TB, Butcher RJ, Wang G, Yee GT (2006) Inorg Chem 45:3023–3033
28. Jia Q-X, Tian H, Yan L, Ma Y, Gao E-Q (2010) Inorg Chim Acta 363:3750–3756
29. Snejko N, Gutiérrez-Puebla E, Martínez JL, Monge MA, Ruiz-Valero C (2002) Chem Mater 14:1879–1883
30. Daumann LJ, Comba P, Larrabee JA, Schenk G, Stranger R, Cavigliasso G, Gahan LR (2013) Inorg Chem 52:2029–2043
31. Su F, Lu L, Feng S, Zhu M (2014) CrystEngComm 16:7990–7999
32. Ma L-F, Wang L-Y, Lu D-H, Batten SR, Wang J-G (2009) Cryst Growth Des 9:1741–1749
33. Zang S-Q, Cao L-H, Liang R, Hou H-W, Mak TCW (2012) Cryst Growth Des 12:1830–1837
34. Huang F-P, Tian J-L, Gu W, Liu X, Yan S-P, Liao D-Z, Cheng P (2010) Cryst Growth Des 10:1145–1154